CHAPTER 7

MECHANICAL AND ELECTROCHEMICAL BEHAVIOR OF ($Fe_{70}Ni_{30}$)-ZrO_2 METAL MATRIX COMPOSITES PREPARED FROM NANO ($Fe_{70}Ni_{30}$) ALLOY AND NANO ZrO_2 POWDERS

In the previous chapter 6, synthesis of $Fe_{(100-x)}Ni_{(x)}$ (where x= 10, 30 and 50 mole%) nanocrystalline alloy powders by using sol-gel autocombustion route and its characterization is described. It is expected that the use of nanosize alloy powder will help in improving mechanical and corrosion properties of the (Fe-Ni)-ZrO_2 metal matrix composites. $Fe_{70}Ni_{30}$ composition was selected for the composite synthesis. ZrO_2 nano particles were used as reinforcement phase to be mixed with the obtained $Fe_{70}Ni_{30}$ nano powder. Compaction of the well mixed powder was followed by sintering in an atmosphere controlled furnace at 900°C/1h. Phase, microstructure, density, hardness and corrosion properties of the prepared composites were examined. The detailed synthesis process is already described in chapter 3 (Section 3.2.2). Flow chart of synthesis flow diagram is shown in Fig. 7.1. Five different compositions with different ZrO_2 content viz. 0, 2.5, 5, 10 and 15 wt.% were prepared and named as A-($Fe_{70}Ni_{30}$), A-($Fe_{70}Ni_{30}$)-2.5ZrO_2, A-($Fe_{70}Ni_{30}$)-5ZrO_2, A-($Fe_{70}Ni_{30}$)-10ZrO_2, A-($Fe_{70}Ni_{30}$)-15ZrO_2, respectively.

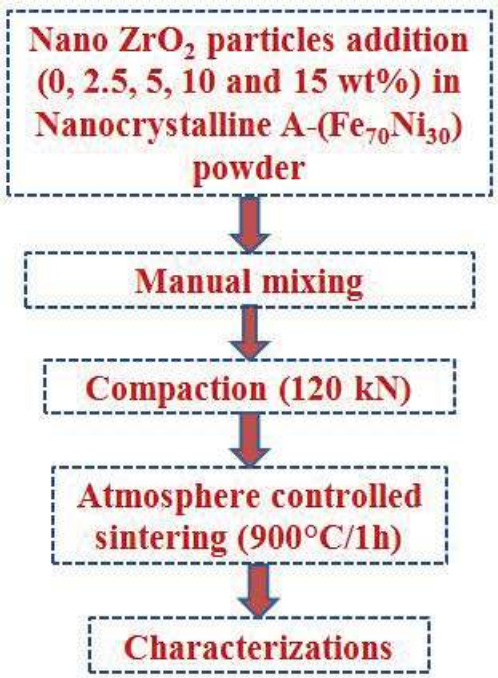

FIGURE 7.1: Flow chart for synthesis of A-($Fe_{70}Ni_{30}$)-ZrO_2 metal matrix composites.

7.1 X-ray Diffraction (XRD)

Fig. 7.2 shows X-ray diffraction patterns of sintered specimens containing (a)0, (b)2.5, (c)5, (d)10 and (e)15 wt.% ZrO_2 nanoparticles as reinforcement phase. In the XRD pattern of 0 wt.% ZrO_2 containing specimen A-($Fe_{70}Ni_{30}$), peaks of γ-(Fe,Ni) and α-(Fe,Ni) are observed. In the remaining sintered specimens (Fig. 7.2b-e), resulting XRD patterns contain three phases i.e. γ-(Fe,Ni), α-(Fe,Ni), and ZrO_2. Peaks were matched with standard JCPDS files.γ-(Fe,Ni) (JCPDS 47-1405), α-(Fe,Ni) (JCPDS 37-0474), and ZrO_2 (JCPDS 78-0047). It is observed that increasing the ZrO_2 content has resulted in the increased ZrO_2 peak intensities. Maximum peak intensity of ZrO_2 is observed in A-($Fe_{70}Ni_{30}$)-15ZrO_2 composite.

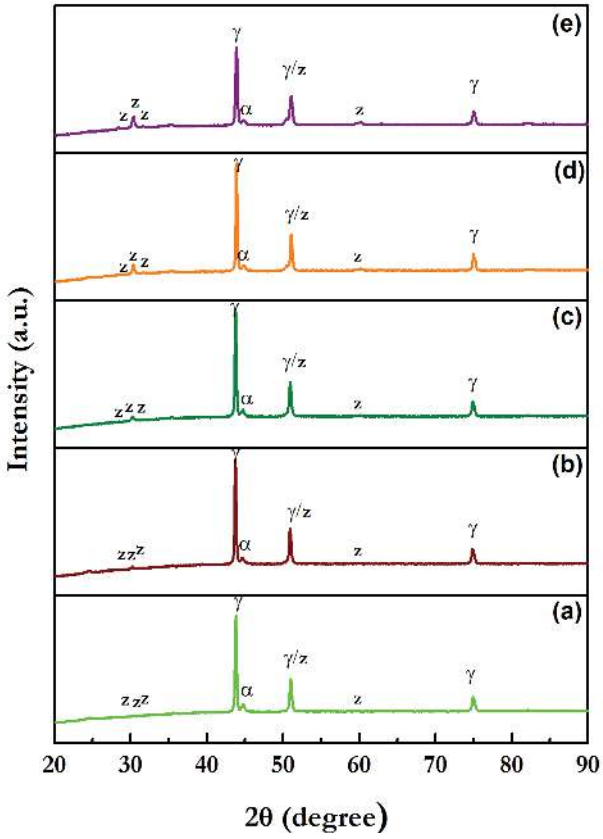

FIGURE 7.2: X-ray diffraction pattern of (a)A-($Fe_{70}Ni_{30}$) (b)A-($Fe_{70}Ni_{30}$)-2.5ZrO_2 (c)A-($Fe_{70}Ni_{30}$)-5ZrO_2 (d)A-($Fe_{70}Ni_{30}$)-10ZrO_2 (e)A-($Fe_{70}Ni_{30}$)-15ZrO_2 composites. (γ- γ-(Fe,Ni); α- α-(Fe,Ni) and z-ZrO_2).

7.2 Microstructure Evolution

Fig. 7.3 shows the backscattered SEM images of (a)A-($Fe_{70}Ni_{30}$) (b)A-($Fe_{70}Ni_{30}$)-2.5ZrO_2 (c)A-($Fe_{70}Ni_{30}$)-5ZrO_2 (d)A-($Fe_{70}Ni_{30}$)-10ZrO_2 (e)A-($Fe_{70}Ni_{30}$)-15ZrO_2 composites. It is observed from resulting micrographs that two regions with different contrast exist in case of A-($Fe_{70}Ni_{30}$) specimen (Fig. 7.3a). Bright region is expected to conain γ-(Fe,Ni) and dark region is expected to contain α-(Fe,Ni) phase along with fine pores. The presence of similar phases was also confirmed from XRD results. Rest of the (Fe,Ni)-ZrO_2

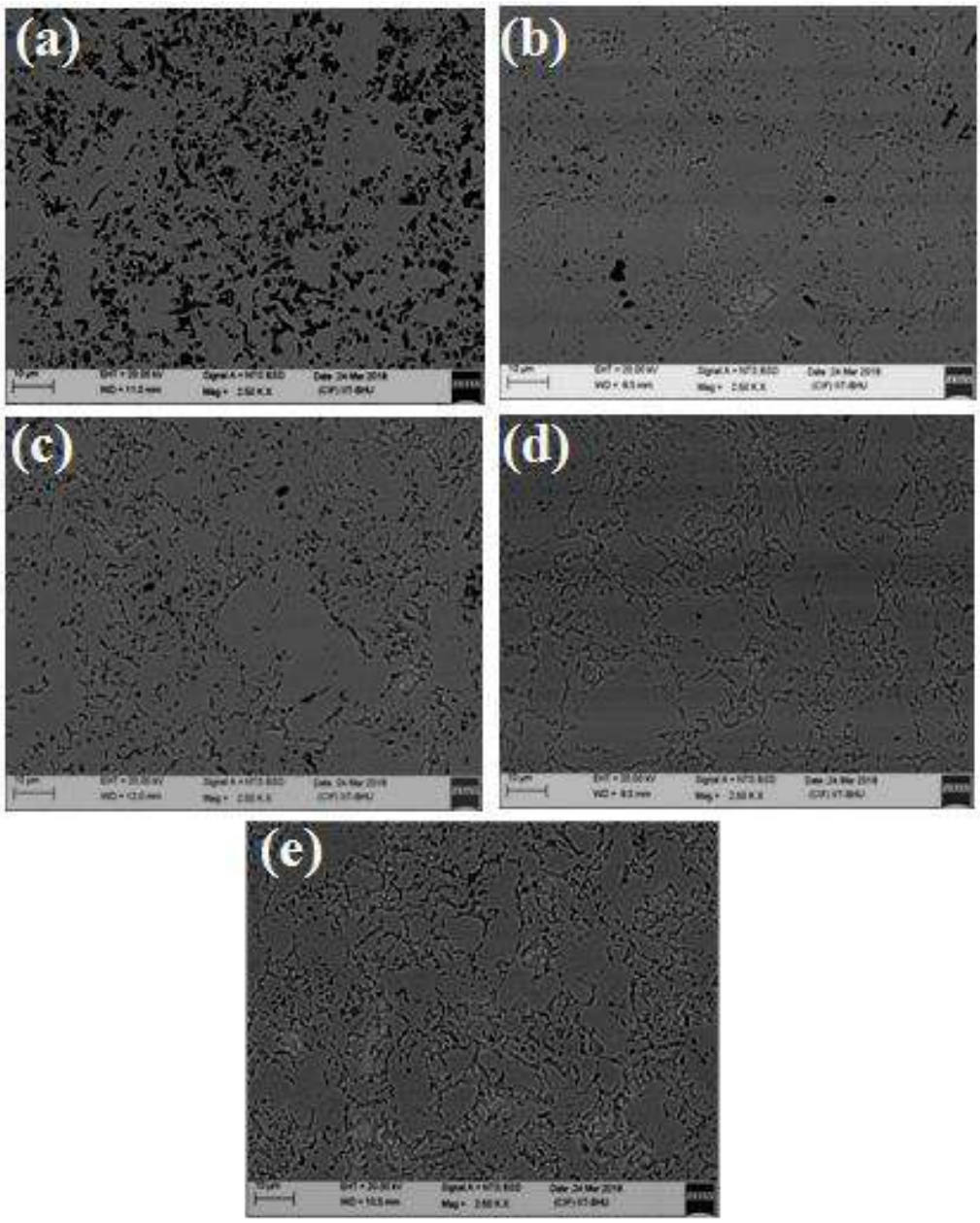

FIGURE 7.3: Back scattered SEM micrographs of (a) A-($Fe_{70}Ni_{30}$)-2.5ZrO_2 (b) A-($Fe_{70}Ni_{30}$)-5ZrO_2 (c) A-($Fe_{70}Ni_{30}$)-10ZrO_2 (d) A-($Fe_{70}Ni_{30}$)-15ZrO_2 specimen surfaces at 2500X magnification.

composites with 2.5, 5, 10 and 15 wt.% ZrO_2 content were found to contain ZrO_2 peaks along with γ and α phases in XRD patterns. From SEM images, ZrO_2 particles are observed to be segregated at the boundary region. The increase in ZrO_2 particles segregation is observed with increasing ZrO_2 content which is found maximum for the composite containing 15 wt.% ZrO_2 content.

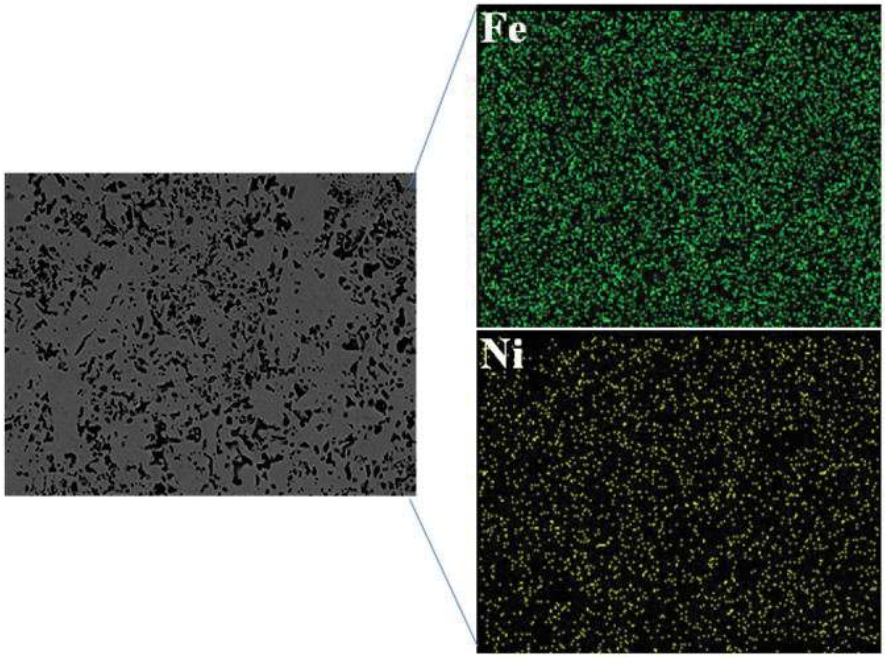

FIGURE 7.4: Elemental mapping of A-($Fe_{70}Ni_{30}$).

Fig. 7.4 shows the elemental mapping of A-($Fe_{70}Ni_{30}$) specimen. It has been observed that the dark region present in the microstructure consists of α phase with more Fe and less Ni elements. At some dark points, absence of both Fe and Ni is observed which are expected to be fne pores. In the bright region, both Fe and Ni are distributed in a significant amount. Fig. 7.5 shows the elemental mapping of A-($Fe_{70}Ni_{30}$)-10ZrO_2 specimen. The white particles were found to contain Zr and O elements. Thus the segregation of ZrO_2 particles at boundary regions is confirmed from elemental mapping. The amount

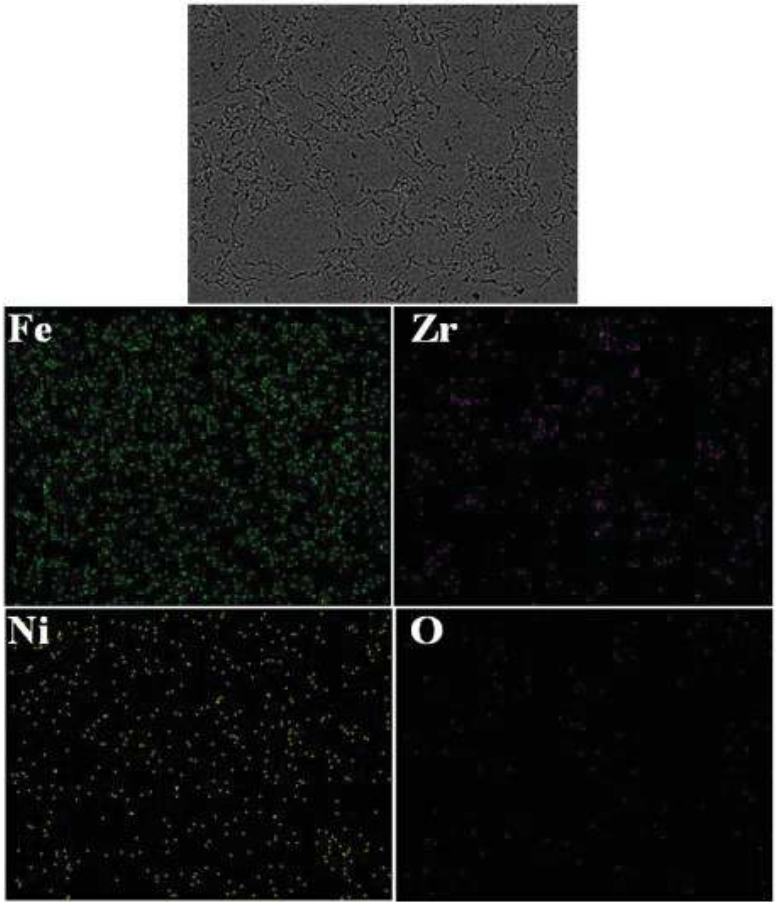

FIGURE 7.5: Elemental mapping of A-($Fe_{70}Ni_{30}$)-10ZrO_2.

of these white particles has increased with increasing ZrO_2 concentration in the specimens. This is in conformity with the XRD and SEM micrographs. There is no evidence of the intermediate phase formation between metal and ceramic phase, and all the phases can be distinguished in XRD patterns. An increase in ZrO_2 peak intensities in XRD and their presence at the pores and boundaries in SEM images support the elemental mapping results. The ZrO_2 particles segregation at pores and boundaries is expected to influence both the mechanical and corrosion behavior of the composites which will be discussed in the further sections.

7.3 Density

Fig. 7.6 shows the density plot of A-($Fe_{70}Ni_{30}$)-ZrO_2 composites with varying ZrO_2 content. It can be observed that there is a decrease in the density with the addition of ZrO_2 particles. For A-($Fe_{70}Ni_{30}$) specimen, density is around 6.77 gm/cm^3 which has decreased to 6.7 gm/cm^3 for composite containing 2.5 wt.% ZrO_2 particles. The addition of 5 and 10 wt.% ZrO_2 in the matrix again resulted in decreased density, i.e., 6.65 and 6.57 gm/^{3} respectively. For 15 wt.% ZrO_2 containing composite specimen, the density is 6.45 gm/cm^3. Theoretical density of ZrO_2 is less as compared to metal phase. Therefore, the addition of

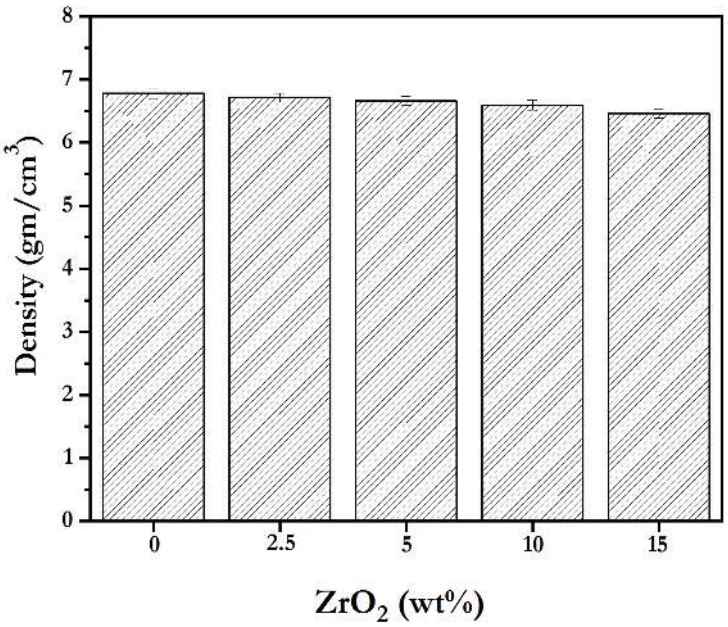

FIGURE 7.6: Density plot of sintered composites with varying ZrO_2 content.

ZrO_2 particles resulted in a decrease in the sintered density of composites. The improvement in solid phase sintering ability of metals results due to the elemental diffusion at the higher sintering temperature. It results in densification and phase formation. In this work,

α and γ-(Fe,Ni) formation in the matrix phase has occurred due to diffusion of Fe and Ni at the sintering temperature. As ZrO_2 particles have a very high melting temperature and strong ionic bonding, therefore, they have not participated in any intermediate phase formation. But because they have a lower density than the matrix phase, this reduced the density of ZrO_2 reinforced composites.

7.4 Hardness

Fig. 7.7 shows the variation of hardness in the composites with an increase in ZrO_2 reinforcement content. It is observed that there is an increase in the hardness value with the addition of ZrO_2 particles. The specimen A-($Fe_{70}Ni_{30}$) with 0 wt.% ZrO_2 content shows the hardness around 118 Hv. When 2.5 wt.% ZrO_2 particles have been added in A-($Fe_{70}Ni_{30}$) composition, the hardness increases to 121 Hv. Addition of 5 and 10 wt.% ZrO_2 content resulted in 130 Hv and 141 Hv hardness, respectively. The maximum hardness was found in 15 wt.% ZrO_2 containing composite having 158 Hv hardness value. For the metal specimen A-($Fe_{70}Ni_{30}$) with 0 wt.% ZrO_2 content, the indentation during hardness results in plastic deformation. It results in a reduction of the hardness of the specimen. Addition of hard ZrO_2 particles retards the plastic deformation and provides support to the soft metal region during indentation. This helps in increasing the hardness of ZrO_2 reinforced composites. As the concentration of ZrO_2 particles is increased, the hardness, therefore, increases and becomes maximum for A-($Fe_{70}Ni_{30}$)-15ZrO_2 composite.

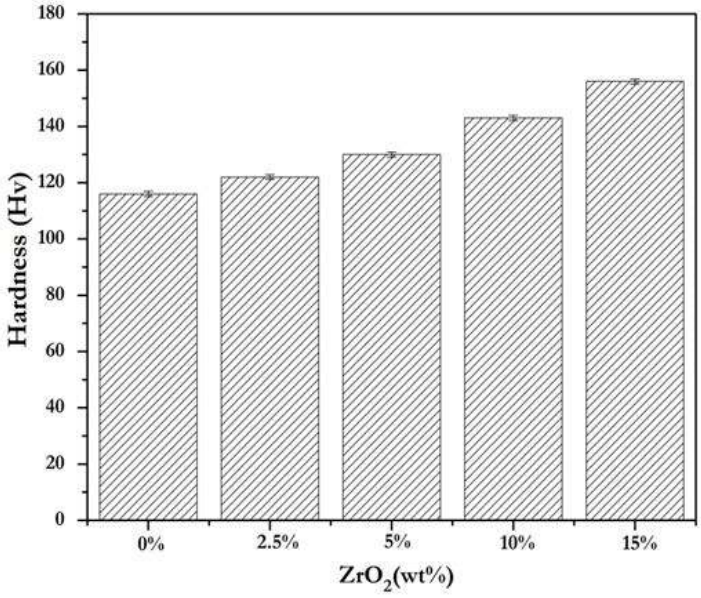

FIGURE 7.7: Hardness plot of sintered composites with varying ZrO_2 content.

7.5 Scanning Kelvin Probe Force Microscopy (SKPFM)

Fig. 7.8 (a-d) shows the volta potential of specimen surfaces observed through in-situ AFM (Atomic Force Microscope). The results show a difference in the surface potential between different phases. From the line scan, it is observed that the volta potential difference is positive at some places whereas it is negative at another place. Presence of ZrO_2 particles shows an influence on the microstructure. Fig. 7.8 (a-b) and (c-d) shows the SKPFM image of A-($Fe_{70}Ni_{30}$) and A-($Fe_{70}Ni_{30}$)-10ZrO_2 composites, respectively. For specimen A-($Fe_{70}Ni_{30}$) with no ZrO_2 content, the potential difference of -8 to -11 mV is at anodic region. At the cathodic region, 5 to 7 mV potential difference is observed. In Fig. 7.8 (c-d), a decrease in potential difference for A-($Fe_{70}Ni_{30}$)-10ZrO_2 composite is observed. The potential value 5 to 6 mV is observed at cathode and -12 to -15mV is observed at anode. This decrease in potential difference is observed due to the presence of

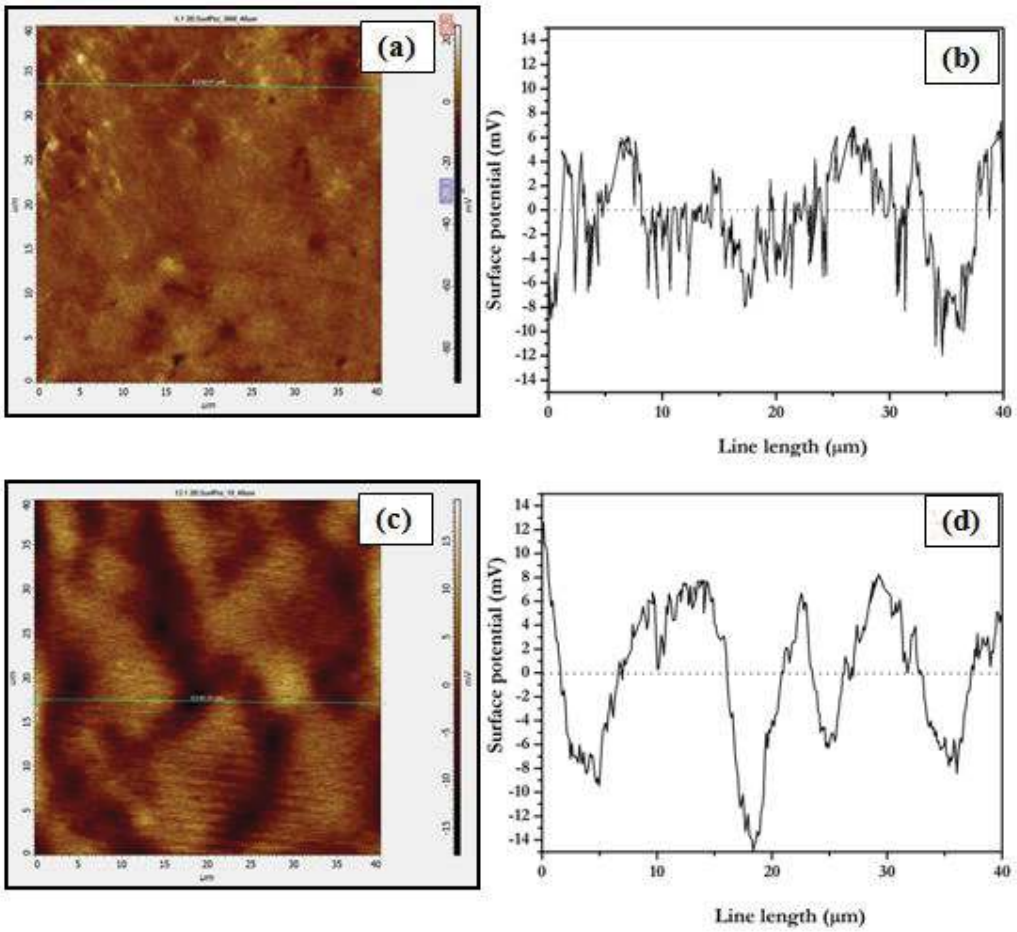

FIGURE 7.8: Surface potential of specmens (a-b) A-($Fe_{70}Ni_{30}$) and (c-d) A-($Fe_{70}Ni_{30}$)-10ZrO_2.

inert ZrO_2 particles. In specimen A-($Fe_{70}Ni_{30}$) surface, the potential difference of surface is decreased as compared to A-($Fe_{70}Ni_{30}$). The decrease in potential difference between cathode and anode region is expected to be helpful in improving the corrosion resistance of composites.

TABLE 7.1: Electrochemical parameters obtained from potentiodynamic polarization curves.

S.No.	Specimen Name	$E_{corr}(mV)$	$I_{corr}(\mu A/cm^2)$	C_r(mpy)	$\mu_p\%$
1	A-($Fe_{70}Ni_{30}$)	-455	30.0	32.4	72
2	A-($Fe_{70}Ni_{30}$)-2.5ZrO_2	-346	26.1	31.0	75.8
3	A-($Fe_{70}Ni_{30}$)-5ZrO_2	-337	23.7	29.1	78.0
4	A-($Fe_{70}Ni_{30}$)-10ZrO_2	-333	17.3	19.5	83.9
5	A-($Fe_{70}Ni_{30}$)-15ZrO_2	-298	7.1	8.3	92.3

7.6 Electrochemical Behavior

7.6.1 Potentiodynamic Polarization Measurements

The electrochemical behavior of the prepared specimens was investigated by potentiodynamic polarization measurement using Tafel extrapolation technique. The kinetics of the corrosion reaction can be obtained from the shape of polarization curves. The polarization curves for different synthesized specimens were recorded after 1h of electrode immersion in 3.5 wt.% NaCl solution at room temperature (Fig. 7.9). It can be observed that the nature of the polarization curve for the ZrO_2 reinforced composites are similar to that of A-($Fe_{70}Ni_{30}$). It is also observed from the plots that the polarization curves for A-($Fe_{70}Ni_{30}$ shows more negative corrosion potential -455 mV. Addition of ZrO_2 results in shifting the corrosion potential towards more positive values. The most positive value is observed for 15% ZrO_2 containing composite.

On comparing the data recorded in Table. 7.1, It is observed that the corrosion current density decreases for ZrO_2 reinforced composites as compared to A-($Fe_{70}Ni_{30}$). The corrosion resistance of the composite specimens is found to improve with increasing the reinforcement content being minimum for the composite containing 15 wt.% ZrO_2. The

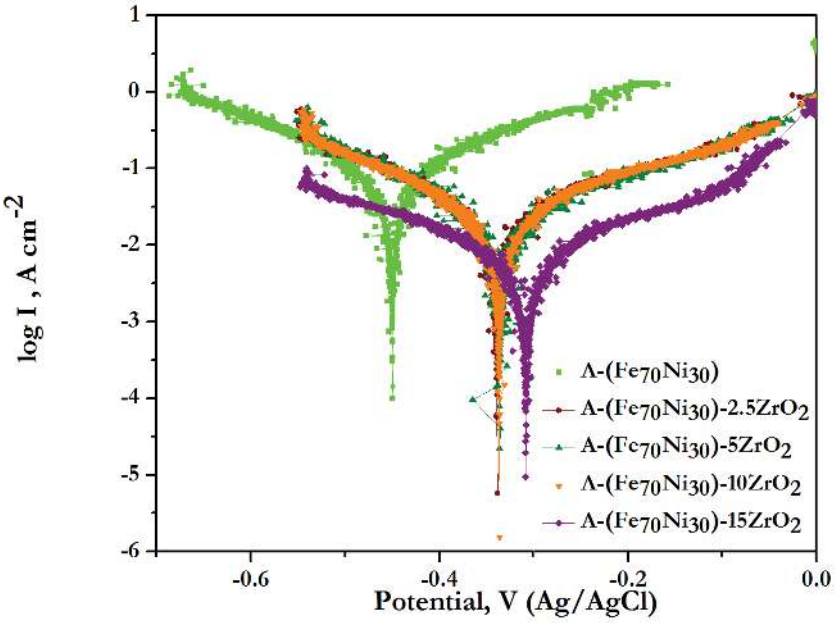

FIGURE 7.9: Tafel polarization plots of specimens in 3.5% NaCl solution.

basic corrosion reactions for the A-($Fe_{70}Ni_{30}$) system in 3.5% NaCl solution is supposed to occur due to the presence of iron-rich phase in the material. Values of corrosion current density decreases from 30.0 μA/cm^2 for A-($Fe_{70}Ni_{30}$) to 26.1 μA/cm^2 for 2.5% ZrO_2 reinforced composite. I_{corr} further decreases to 23.7 μA/cm^2 for 5% ZrO_2 and 17.3 μA/cm^2 for 10 wt.% reinforced composites. This improvement in the performance of the composite may be due to the incorporation of the ZrO_2 particles in the metal matrix. Minimum I_{corr} i.e. 7.1 μA/cm^2 is observed for composites containing 15wt.% ZrO_2. It is inferred that the addition of inert oxide (ZrO_2) as a reinforcement diminishes the density of active sites on the metal surface and the amount of these active sites decreases with increasing ZrO_2 content. The improved performance of a metal or alloy due to the incorporation of

non-metallic particles is reported in case of coating materials [124]. It is believed that the metal surface possesses defects, gaps, crevices and holes and the ZrO_2 particles fill these defects, slowing down the dissolution of the metal through these active sites. During the initial oxidation period, a protective iron hydroxide layer is formed which becomes more and more compact with an increase in zirconia content and consequently the corrosion resistance against the attack of Cl- ion is improved.

7.6.2 Electrochemical Impedance Spectroscopy analysis

Fig. 7.10 shows the Nyquist plots for specimens examined in 3.5% NaCl solution. It can be observed that the impedance responses was significantly changed for the ZrO_2 reinforced composites relative to that of A-($Fe_{70}Ni_{30}$) specimen. In case of A-($Fe_{70}Ni_{30}$), one very small capacitive loop is observed at high frequency followed by a big capacitive loop (Fig. 7.10 a). The EIS data has been fitted to appropriate equivalent circuits to properly interpret the results. The Nyquist plot at lower frequency range is shown in Fig. 7.10 (b) from which the nature of circuit can be clearly observed. The EC for A-($Fe_{70}Ni_{30}$) is shown as an inset in Fig. 7.10 (a) which contains one pure resistive part (R_1) that represents the resistance between working and reference electrode. This is in series with (Q_2), the constant phase element (CPE) which represents the capacitance in parallel with a resistance (R_2).

This is for the charge transfer process of the electrode in the electrolyte system. This circuit contains one additional CR circuit. The additional capacitance and resistance for the alloy system may be due to the presence of two phases, i.e., γ-(Fe,Ni) and α-(Fe,Ni).

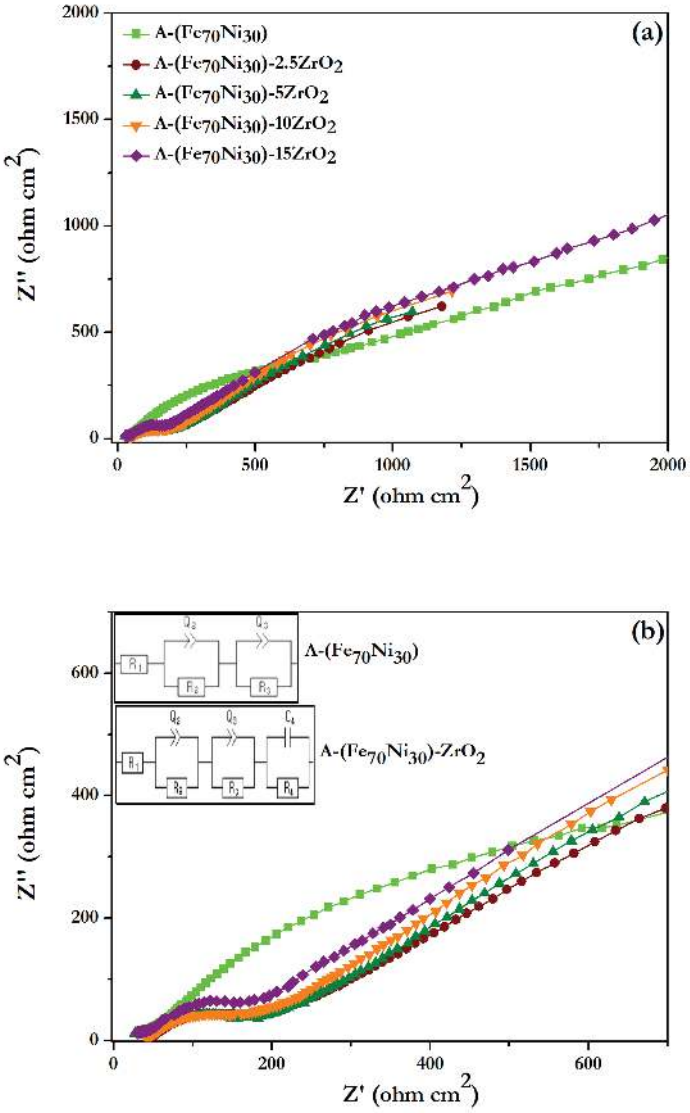

FIGURE 7.10: Nyquist plots (a) obtained for prepared composites with equivalent circuit (b) plots after zooming at lower frequency.

In the XRD results (Fig. 7.2), it has already been discussed that the A-($Fe_{70}Ni_{30}$) specimen contains γ-(Fe,Ni) phase in addition to α-(Fe,Ni) and thereby the electrolyte faces two types of grains at the electrode surface. The EC for the ZrO_2 reinforced composites comprise three CR circuits as shown in Fig. 7.10 (a). Unlike A-($Fe_{70}Ni_{30}$), the third CR

circuit for the composite specimens may be due to the presence of ZrO_2 reinforcement in the metal matrix. The ZrO_2 particles are imagined to be embedded in the host matrix and blocking the path of the charge carriers to the electrode system. This means that the active sites for the corrosion process are blocked. Accordingly, it is noted that the diameters of the circular arcs have increased for the composite materials in comparison to A-($Fe_{70}Ni_{30}$) specimen. This shows that the composite material is more corrosion resistant as compared to A-($Fe_{70}Ni_{30}$) specimens. This may be because the increase in the concentration of the zirconia causes the increase in the number of the blocking of the active sites for the corrosion process.

7.6.3 Scanning electron micrographs after corrosion

Fig. 7.11 shows the SEM micrographs of the corroded surfaces after potentiodynamic polarization measurements in NaCl solution. After corrosion test, it has been observed that the surface of the A-($Fe_{70}Ni_{30}$) specimen has been affected more than the ZrO_2 reinforced composites. Addition of ZrO_2 A-($Fe_{70}Ni_{30}$) surface, the presence of ZrO_2 particles in the matrix have helped in resisting corrosion at the surface. Increasing ZrO_2 content from 2.5 to 10 wt.%, corrosion resistance is improved which is evident from the Tafel plots, and impedance data and hence the electrolyte has not much affected the specimen surface.

From the micro graph, A-($Fe_{70}Ni_{30}$)-15ZrO_2 has been found to have least affected surface. It is already mentioned that the ZrO_2 particles have segregated at the boundary region and pits, improved the composite surface. Therefore the presence of these inert

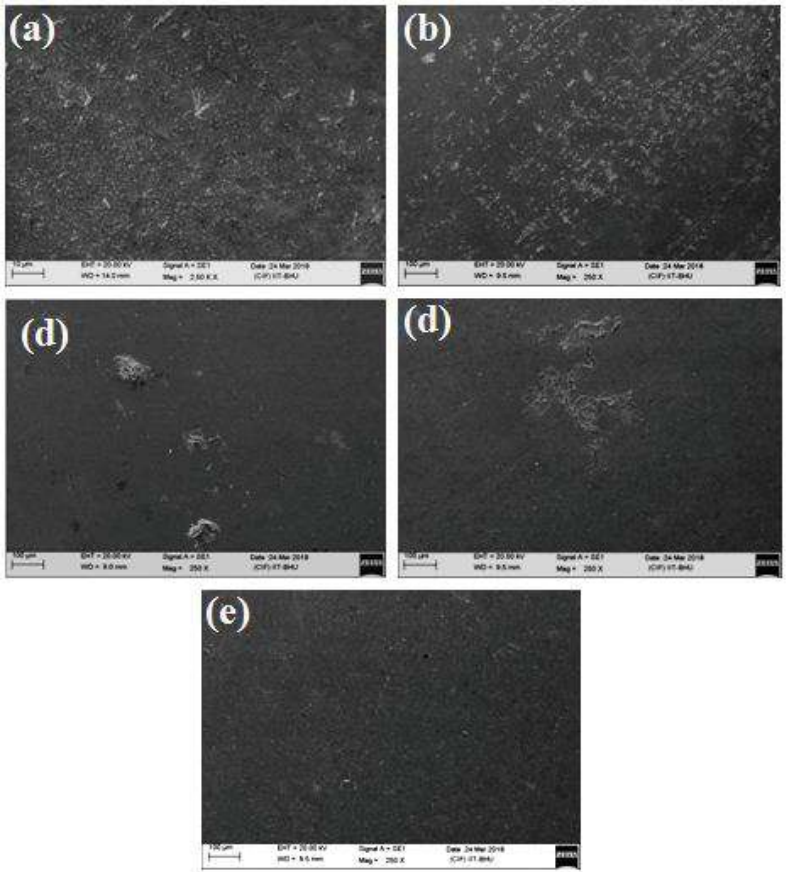

FIGURE 7.11: SEM micrographs of specimen surfaces (a) A-($Fe_{70}Ni_{30}$) (b) A-($Fe_{70}Ni_{30}$)-2.5ZrO_2 (c) A-($Fe_{70}Ni_{30}$)-5ZrO_2 (d) A-($Fe_{70}Ni_{30}$)-10ZrO_2 (f) A-($Fe_{70}Ni_{30}$)-15ZrO_2 specimens after corrosion test at 250X magnification.

particles at high energy region has reduced the attack from electrolyte solution and have developed the corrosion resistance.

7.7 Summary of the chapter

Addition of nano ZrO_2 particles with chemically synthesized $Fe_{70}Ni_{30}$ nano powder is done. The compaction of the well-mixed powder was followed by sintering in an atmosphere controlled furnace at 900°C/1h. Phase, microstructure, density, hardness and

corrosion properties of the prepared composites were examined. XRD patterns show the presence of γ-(Fe,Ni), α-(Fe,Ni) and ZrO_2 peaks in sintered composites. Segregation of nano ZrO_2 particles is observed at the pore and boundary region in the micrographs. Maximum density is achieved in A-($Fe_{70}Ni_{30}$) sintered specimen. Addition of ZrO_2 particles resulted in a slight decrease in density of composite. Maximum hardness 155 Hv is observed in the composite containing 15 wt.% ZrO_2 content. For the composites A-($Fe_{70}Ni_{30}$)-ZrO_2, the presence of nanoparticles at grain boundaries and pores results in enhanced corrosion resistance.